2. FULL–LENGTH ARTICLE

BEYOND THE FRACTAL

Sandra Lach Arlinghaus

"I never saw a moor,
I never saw the sea;
Yet know I how the heather looks,
And what a wave must be."

Emily Dickinson, "Chartless."

Abstract.

The fractal notion of self-similarity is useful for characterizing change in scale; the reason fractals are effective in the geometry of central place theory is because that geometry is hierarchical in nature. Thus, a natural place to look for other connections of this sort is to other geographical concepts that are hierarchical in nature. Within this fractal context, this chapter examines the case of spatial diffusion.

When the idea of diffusion is extended to see "adopters" of an innovation as "attractors" of new adopters, a Julia set is introduced as a possible axis against which to measure one class of geographic phenomena. Beyond the fractal context, fractal concepts, such as "compression" and "space- filling" are considered in a broader graph–theoretic context.

Introduction.

Because a fractal may be considered as a randomly generated statistical image (Mandelbrot, 1983), one place to look for geometric fractals tailored to fit geographic concepts is within the set of ideas behind spatial configurations traditionally characterized using randomness. The spatial diffusion of an innovation is one such case; Hägerstrand characterized it using probabilistic simulation techniques (Hägerstrand, 1967). This chapter builds directly on Hägerstrand's work in order to demonstrate, in some detail, how fractals might arise in spatial diffusion. From there, and with a view of an adopter of an innovation as an "attractor" of other adopters, the connected Julia set $z = z^2 - 1$ is examined, only broadly, for its potential to serve as an axis from which to measure spatial "attraction."

More generally, it is not necessary to consider fractal– like concepts such as "attraction," "space–filling," or "compression" relative to any metric, as in the diffusion example, or relative to any axis, as in the Julia set case. These broad fractal notions are examined, in some detail, in a graph–theoretic realm, free from metric/axis encumbrance, as one step beyond the fractal. An effort has been made to explain key geographical and mathematical concepts so that much of the material, and the flow of ideas, is self- contained and accessible to readers from various disciplines.

A fractal connection to spatial diffusion

The diffusion of the knowledge of an innovation across geographic space may be simulated numerically using Monte Carlo techniques based in probability theory (Hägerstrand, 1967). A simple example illustrates the basic mechanics of Hägerstrand's procedure.

Consider a geographic region and cover it with a grid of uniform cell size suited to the scale of the available empirical information about the innovation. Enter the number of initial adopters of the innovation in the grid: an entry of "1" means one person (household, or other

set of people) knows of the innovation. Over time, this person will tell others. Assume that the spread of the news, from this person to others, decays with distance. To simulate this spread, probabilities of the likelihood of contact will be assigned to each cell surrounding each initial adopter. A table of random numbers is used in conjunction with the probabilities, as follows.

Given a gridded geographic region and a distribution of three initial adopters of an innovation (Figure 1). Assume that an initial telling occurs no more than two cells away from the initial adopters' cells. This assumption creates a five–by–five grid in which interchange can occur between an initial adopter in the central cell and others. Assign probabilities of contact to each of these twenty–five cells as a percentage likelihood that a randomly chosen four digit number falls within a given interval of numbers assigned to each cell (Figure 2). Because the intervals in Figure 2 partition the set of four digit numbers, the percentage probabilities assigned to each cell add to 100%. Pick up the five–by–five grid and center it on the original adopter in cell H3 (Figure 1). Choose the first number, 6248, in the list of random numbers (Figure 2). It falls in the interval of numbers in the central cell. Enter a "+1" in the associated cell, H3, to represent this new adopter. Move the five–by– five grid across the distribution of original adopters, stopping it and repeating this procedure with the next random number in the list each time a new original adopter is encountered. Center the five–by–five grid on H4; the next random number is 0925 which falls in the interval in the cell immediately northwest of center (Figure 2). Enter a "+1" in cell G3 (Figure 1), the cell immediately northwest of H4. Finally, center the moving grid on H5. The next random number, 4997, falls in the center cell; therefore, enter a "+1" in cell H5. Once this procedure has been applied to all original adopters, the population of adopters doubles and a "first generation" of adopters, comprising original adopters and newer adopters represented as "+1's", emerges (Figure 1). Any number of additional generations of adopters of the innovation may be simulated by iteration of this procedure.

There are numerous side issues, which are important, that may complicate this basic procedure (Hägerstrand, 1967; Haggett *et al.*, 1977). How are the percentages for the five–by–five grid chosen? Indeed, how is the dimension of "five" chosen for a side of this grid? Should the choices of percentages and of dimension be based on empirical data, on other abstract considerations, or on a mix of the two? What sorts of criteria should there be in judging suitability of empirical data? What if a random entry falls outside the given grid; what sorts of boundary/barrier considerations, both in terms of the position of new adopters relative to the regional boundary and of the symmetry of the probabilities within the five–by–five grid, should be taken into account?

Independent of how many generations are calculated using this procedure, the pattern of "filling in" of new adopters is heavily influenced by the shape of the set of original adopters. Indeed, over time, knowledge of the innovation diffuses slowly initially, picks up in speed of transmission, tapers off, and eventually the population becomes saturated with the knowledge. Typically this is characterized as a continuous phenomenon using a differential equation of inhibited growth that has as an initial supposition that the population may not exceed M, an upper bound, and that $P(t)$, the population P at time t, grows at a rate proportional to the size of itself and proportional to the fraction left to grow (Haggett *et al.*, 1977; Boyce

Figure 1.

Three original adopters, represented as 1's. Positions are simulated for three new adopters, represented as +1's. The two sets taken together form a first generation of adopters of an innovation (grid after Hägerstrand).

North at the top.

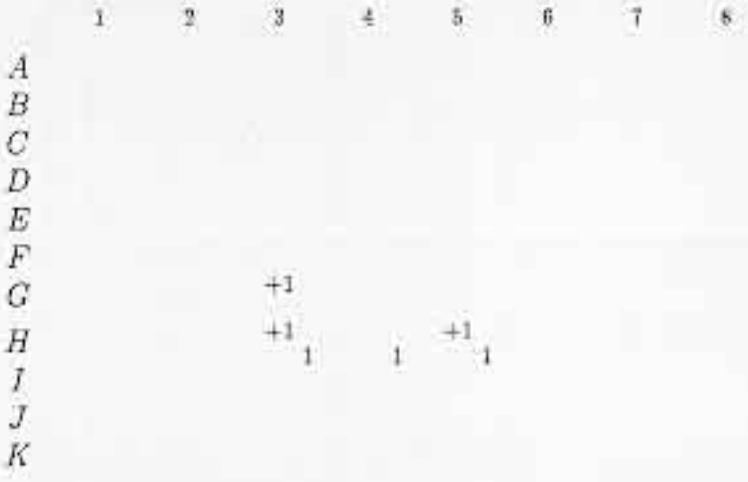

and DiPrima, 1977). An equation such as

$$\frac{dP(t)}{dt} = k\,P(t)(1-(P(t)/M))$$

serves as a mathematical model for this sort of growth in which $k > 0$ is a growth constant and the fraction $(1-(P(t)/M)$ acts as a damper on the rate of growth (Boyce and DiPrima, 1977). The graph of the equation is an S–shaped (sigmoid) logistic curve with horizontal asymptote at $P(t) = M$ and inflection point at $P(t) = M/2$. When $dP/dt > 0$ the population shows growth; when $d^2P/dt^2 > 0$ (below $P(t) = M/2$) the rate of growth is increasing; when $d^2P/dt^2 < 0$ (above $P(t) = M/2$) the rate of growth is decreasing.

The differential equation model thus yields information concerning the rate of change of the total population and in the rate of change in growth of the total population. It does not show how to determine M; the choice of M is given *a priori*.

Iteration of the Hägerstrand procedure gives a position for M once the procedure has been run for all the generations desired.

For, it is a relatively easy matter to accumulate the distributions of adopters and stack them next to each other, creating an empirical sigmoid logistic curve based on the simulation (Haggett *et al.*, 1977). Finding the position for the asymptote (or for *an* upper bound close to the asymptotic position) is then straightforward.

Neither the Hägerstrand procedure nor the inhibited growth model provides an estimate of saturation level (horizontal asymptote position) (Haggett, *et al.*, 1977) that can be calculated early in the measurement of the growth. The fractal approach suggested below offers a means for making such a calculation when self-similar hierarchical data are involved; allometry is a special case of this procedure (Mandelbrot, 1983). The reasons for wanting to

Figure 2.

Five–by–five grid overlay. Numerical entries in cells show the percentage of four digit numbers associated with each cell. The given listing of cells shows which cell is associated with which range of four digit numbers.

North at the top.

	1	2	3	4	5
1	0.96	1.40	1.68	1.40	0.96
2	1.40	3.01	5.47	3.01	1.40
3	1.68	5.47	44.31	5.47	1.68
4	1.40	3.01	5.47	3.01	1.40
5	0.96	1.40	1.68	1.40	0.97

A random set of numbers (source: *CRC Handbook of Standard Mathematical Tables*):
6248, 0925, 4997, 9024, 7754
7617, 2854, 2077, 9262, 2841
9904, 9647,
and so forth.

Random number assignment to matrix cells, with cell number given as an ordered pair whose first entry refers to the reference number on the left of the matrix in this figure and whose second entry refers to the reference number at the top of that matrix.

(1,1): 0000-0095; (1,2): 0096-0235; (1,3): 0236-0403
(1,4): 0404-0543; (1,5): 0544-0639
(2,1): 0640-0779; (2,2): 0780-1080; (2,3): 1081-1627
(2,4): 1628-1928; (2,5): 1929-2068
(3,1): 2069-2236; (3,2): 2237-2783; (3,3): 2784-7214
(3,4): 7215-7761; (3,5): 7762-7929
(4,1): 7930-8069; (4,2): 8070-8370; (4,3): 8371-8917
(4,4): 8918-9218; (4,5): 9219-9358
(5,1): 9359-9454; (5,2): 9455-9594; (5,3): 9595-9762
(5,4): 9763-9902; (5,5): 9903-9999

make such a calculation might be to determine where to position adopter "seeds" in order to produce various levels of innovation saturation.

As is well–known, not all innovations diffuse in a uniform manner; Paris fashions readily available in major U. S. cities up and down each coast might seldom be seen in rural midwestern towns. To determine how the ideas of fractal "space–filling" and this sort of diffusion–related "space- filling" might be aligned, consider the following example.

Given a distribution of three original adopters occupying cells H3, H4, and H5 in a linear pattern (Figure 3.A). The probabilities for positions for new adopters are encoded within each cell surrounding each of these (as determined from the five–by–five grid of Figure 2).

Figure 3.A.

The simulation is run on three original adopters with positions given below. Numerical entries show the likelihood, out of 300, that a new adopter will fall into a given cell. Zones of interaction between overlapping five–by–five grids are outlined by a heavy line (begin at the upper left–hand corner (ulhc) of cell F2; move horizontally to the upper right–hand corner (urhc) of cell F6; vertically to lower right–hand corner (lrhc) of cell J6; horizontally to lower left–hand corner (llhc) of cell J2; vertically to ulhc of F2 — should be a rectangular enclosure that you have added to this figure). **Original adopters are in cells H3, H4, H5.**

North at the top.

	1	2	3	4	5	6	7	8	*Totals*
A									
B									
C									
D									
E									
F	0.96	2.36	4.04	4.48	4.04	2.36	0.96		19.20
G	1.40	4.41	9.88	11.49	9.88	4.41	1.40		42.87
H	1.68	7.15	51.46	55.25	51.46	7.15	1.68		175.83
I	1.40	4.41	9.88	11.49	9.88	4.41	1.40		42.87
J	0.96	2.36	4.04	4.48	4.04	2.36	0.96		19.20
K									
	6.40	20.69	79.30	87.19	79.31	20.70	6.41		300

Thus, for example, when the grid of Figure 2 is superimposed and centered on the original adopter in cell H3, a probability of 3.01% is assigned to the likelihood for contact from H3 to G4; when it is superimposed and centered on the original adopter in H4, there is a 5.47% likelihood for contact from H4 to G4; and, when it is superimposed and centered on the original adopter in H5, there is a 3.01% likelihood for contact from H5 to G4. Therefore, the percentage likelihood of a new first–generation adopter in cell G4, given this initial configuration of adopters, is the sum of the percentages divided by the number of initial adopters, or 11.49/3. For ease in inserting fractions into the grid, only the numerator, 11.49, is shown as the entry (Figure 3.A). It would be useful, for purposes of comparison of this distribution to those with sets of initial adopters of sizes other than 3, to divide by the number of initial adopters in order to derive a percentage that is independent of the size of the initial distribution (*i.e.*, to normalize the numerical entries).

It is easy to see that the values in the cells of Figure 3.A must add to a total of 300 if one views them as derived from each of three five–by–five grids centered on each original adopter. A "zone of interaction" of entries from two or more five–by–five grids is outlined by a heavy line; 25 cells are enclosed in it in Figure 3.A. The pattern of numbers exhibits bilateral symmetry, insofar as is possible (allowing for the "appendix" of .01 required to make the numerical partition associated with Figure 2 complete) with respect to both North–South and East–West axes (with the origin in cell H4). Sum and column totals are calculated; as

Figure 3.B.

The simulation is run on three original adopters with positions given below. Numerical entries show the likelihood, out of 300, that a new adopter will fall into a given cell. Zones of interaction between overlapping five-by-five grids are outlined by a heavy line (begin ulhc of F2; horizontally to urhc of F6; vertically to lrhc of I6; horizontally to lrhc of I5; vertically to lrhc of J5; horizontally to llhc of J3; vertically to llhc of I3; horizontally to llhc of I2; vertically to ulhc of F2 — should be a "fat" T-shaped enclosure that you have added to this figure). **Original adopters are in cells H3, G4, H5.**

North at the top.

	1	2	3	4	5	6	7	8	*Totals*
A									
B									
C									
D									
E		0.96	1.40	1.68	1.40	0.96			6.40
F	0.96	2.80	5.65	8.27	5.65	2.80	0.96		27.09
G	1.40	4.69	12.34	50.33	12.34	4.69	1.40		87.19
H	1.68	6.87	49.00	16.41	49.00	6.87	1.68		131.51
I	1.40	3.97	8.27	7.70	8.27	3.98	1.40		34.99
J	0.96	1.40	2.64	2.80	2.65	1.40	0.97		12.82
K									
	6.40	20.69	79.30	87.19	79.31	20.70	6.41		300

the shape of the distribution of initial adopters is altered (below), these totals will tag sets of cells to demonstrate how changes in the zone of interaction are occurring.

Next consider a distribution of three initial adopters derived from the linear one by moving the middle adopter one unit to the North (Figure 3.B). When interaction values are calculated as they were for the initial distribution in Figure 3.A, a comparable, but different numerical pattern emerges (Figure 3.B). Here, the column totals are the same as those in Figure 3.A, but the row totals are different. The zone of interaction contains 23 cells; the highest individual cell value of 50.33 is less than that of the highest cell value, 55.25, in Figure 3.A. Because both sets of values are partitions of the number 300, and because there are more cells with potential for contact in Figure 3.B than in Figure 3.A, the concentration of entries in Figure 3.B is not as compressed as in Figure 3.A. This is reflected in the row totals; a visual device useful for tracking this compression is to think of the five-by-five grid centered on the middle adopter being gradually pulled, to the North, from under the set of entries in Figure 3.A. In Figure 3.B the top of this middle grid slips out from under, failing to intersect the bottom row, J, of the grid. With this view, it is easy to understand why only the row totals, and not the column totals, change.

Naturally, as the middle initial adopter is pulled successively one unit to the north in the configuration of original adopters, the middle five-by-five grid is also pulled one unit to the north (Figures 3.C, 3.D, 3.E, and 3.F). The numerical consequence is to reduce the

Figure 3.C.

The simulation is run on three original adopters with positions given below. Numerical entries show the likelihood, out of 300, that a new adopter will fall into a given cell. Zones of interaction between overlapping five–by–five grids are outlined by a heavy line (begin ulhc of F2; horizontally to urhc of F6; vertically to lrhc of H6; horizontally to lrhc of H5; vertically to lrhc of J5; horizontally to llhc of J3; vertically to llhc of H3; horizontally to llhc of H2; vertically to ulhc of F2 — should be a "less–fat" T–shaped enclosure that you have added to this figure). **Original adopters are in cells H3, F4, H5.**

North at the top.

	1	2	3	4	5	6	7	8	*Totals*
A									
B									
C									
D		0.96	1.40	1.68	1.40	0.96			6.40
E		1.40	3.01	5.47	3.01	1.40			14.29
F	0.96	3.08	8.11	47.11	8.11	3.08	0.96		71.41
G	1.40	4.41	9.88	11.49	9.88	4.41	1.40		42.87
H	1.68	6.43	47.39	12.62	47.39	6.44	1.68		123.63
I	1.40	3.01	6.87	6.02	6.87	3.01	1.40		28.58
J	0.96	1.40	2.64	2.80	2.65	1.40	0.97		12.82
K									
	6.40	20.69	79.30	87.19	79.31	20.70	6.41		300

size of the zone of interaction among the initial adopters and to spread the range of cells over which the value of 300 is partitioned. This implies less concentration near the original adopters and less "filling in" around them as one proceeds from Figure 3.A to Figure 3.F. Thus, in Figure 3.C the zone of interaction shrinks to 21 cells with a largest individual cell entry of 47.39. At the stage shown in Figure 3.D, the largest cell entry is 45.99; because the cells associated with this value are not overlapped by the five–by– five grid centered on the middle adopter, this largest value will not change as the middle adopter is pulled more to the north. Table 1 shows the sizes of the zones of interaction of the largest individual cell entry for each of Figures 3.A to 3.F. No new information arises from moving the middle cell to the north beyond the position in Figure 3.F; the five– by–five grid is revealed and no longer intersects the two overlapping grids associated with the other two initial adopters.

The example depicted in Figure 3 shows that even as early as the first generation, the pattern of the positions of the initial adopters affects significantly the configuration of the later adopters. Figure 3.A with the heaviest possible filling of space using three initial adopters represents a most saturated case, which, taken together with an underlying symmetry that is bilateral relative to mutually perpendicular axes, suggests that an associated space–filling curve should have dimension 2, should have a rectilinear appearance, and should be formed from a generator whose shape is related to the pattern of placement of the original adopters. One space–filling curve that meets these requirements is the rectilinear curve of Figure 4.A.

Figure 3.D.

The simulation is run on three original adopters with positions given below. Numerical entries show the likelihood, out of 300, that a new adopter will fall into a given cell. Zones of interaction between overlapping five–by–five grids are outlined by a heavy line (begin ulhc of F2; horizontally to urhc of F6; vertically to lrhc of G6; horizontally to lrhc of G5; vertically to lrhc of J5; horizontally to llhc of J3; vertically to llhc of G3; horizontally to llhc of G2; vertically to ulhc of F2 — should be a "less–fat" T–shaped enclosure that you have added to this figure). **Original adopters are in cells H3, E4, H5.**

North at the top.

	1	2	3	4	5	6	7	8	*Totals*
A									
B									
C		0.96	1.40	1.68	1.40	0.96			6.40
D		1.40	3.01	5.47	3.01	1.40			14.29
E		1.68	5.47	44.31	5.47	1.68			58.61
F	0.96	2.80	5.65	8.27	5.65	2.80	0.96		27.09
G	1.40	3.97	8.27	7.70	8.27	3.98	1.40		34.99
H	1.68	5.47	45.99	10.94	45.99	5.47	1.68		117.22
I	1.40	3.01	6.87	6.02	6.87	3.01	1.40		28.58
J	0.96	1.40	2.64	2.80	2.65	1.40	0.97		12.82
K									
	6.40	20.69	79.30	87.19	79.31	20.70	6.41		300

The generator is composed of three nodes hooked together by two edges in a straight path. This is scaled–down, by a factor of 1/2, and hooked to the endpoints of the original generator. Iteration of this procedure leads to a rectilinear tree with the desired properties. The approach of looking for a geometric form to fit a given set of conditions is like the calculus approach of looking for a differential equation to fit a given set of conditions. The difference here is that the shape of the generator and other information from early stages may be used to estimate the relative saturation or space–filling level.

The spatial position of the original adopters in Figure 3.B suggests a fractal generator in the shape of a "V" with an interbranch angle, θ, of 90 degrees, while the V in Figure 3.C suggests a generator with $\theta \approx 53°$, that of Figure 3.D one with $\theta \approx 37°$, that of Figure 3.E one with $\theta \approx 28°$, and that of Figure 3.F one with $\theta \approx 23°$. Figures 4.B, 4.C, 4.D, 4.E, and 4.F suggest trees that can be generated using these values for θ.

A rough measure of how much space each one "fills" may be calculated using Mandelbrot's formula for fractal dimension, D, as,

$$D = \frac{\ln N}{\ln (1/r)}$$

where N represents the number of sides in the generator, which in all cases here is the value 2, and where r is some sort of scaling value that remains constant independent of scale

Figure 3.E.

The simulation is run on three original adopters with positions given below. Numerical entries show the likelihood, out of 300, that a new adopter will fall into a given cell. Zones of interaction between overlapping five-by-five grids are outlined by a heavy line (begin ulhc of F2; horizontally to urhc of F6; vertically to lrhc of F6; horizontally to lrhc of F5; vertically to lrhc of J5; horizontally to llhc of J3; vertically to llhc of F3; horizontally to llhc of F2; vertically to ulhc of F2 — should be a "less-fat" T-shaped enclosure that you have added to this figure). **Original adopters are in cells H3, D4, H5.**

North at the top.

	1	2	3	4	5	6	7	8	*Totals*
A									
B		0.96	1.40	1.68	1.40	0.96			6.40
C		1.40	3.01	5.47	3.01	1.40			14.29
D		1.68	5.47	44.31	5.47	1.68			58.61
E		1.40	3.01	5.47	3.01	1.40			14.29
F	0.96	2.36	4.04	4.48	4.04	2.37	0.96		19.21
G	1.40	3.01	6.87	6.02	6.87	3.01	1.40		28.58
H	1.68	5.47	45.99	10.94	45.99	5.47	1.68		117.22
I	1.40	3.01	6.87	6.02	6.87	3.01	1.40		28.58
J	0.96	1.40	2.64	2.80	2.65	1.40	0.97		12.82
K									
	6.40	20.69	79.30	87.19	79.31	20.70	6.41		300

(Mandelbrot, 1977). The difficulty in the case of trees, deriving from the complication of intersecting branches, is to select a suitable description for r. One angle, ϕ, that remains constant throughout the iteration, and that produces the desired effect for the case in which the diffusion is the most saturated, is the base angle of the isoceles triangle with apex angle $\theta/2$ whose equal sides have the length of the equal sides of the two branches of the generator (Figure 5). When r is taken as the cosine of ϕ, then $D = 2$ in the case of Figure 4.A and it decreases dramatically as the trees generated by the distribution of original adopters fill less space (Table 2).

This decreasing sequence of D-values corresponds only loosely to Mandelbrot's measurements of fractal dimensions of trees (Mandelbrot, 1983); here, however, when $D = 1$ the corresponding tree is one with an interbranch angle of 120°. This has some appeal if one notes that then the tree associated with $D = 1$ might therefore represent a Steiner network (tree of shortest total length under certain circumstances) or part of a central place net. The numerical unit D-value would thus correspond to optimal forms for transport networks or for urban arrangements in abstract geographic space (in which Hägerstrand's diffusion procedure also exists).

One use for these D-values, which measure the relative space-filling by trees, might be as units fundamental to developing an algebraic structure for planning the eventual saturation level to arise in communities into which an innovation is introduced to selected adopters. By

Summer, 1990

Figure 3.F.

The simulation is run on three original adopters with positions given below. Numerical entries show the likelihood, out of 300, that a new adopter will fall into a given cell. Zones of interaction between overlapping five-by-five grids are outlined by a heavy line (begin at ulhc of F3, horizontally to urhc of F5, vertically to lrhc of J5; horizontally to llhc of J3; vertically to ulhc of F3 — should be a rectangular enclosure that you have added to this figure). **Original adopters are in cells H3, C4, H5.**

North at the top.

	1	2	3	4	5	6	7	8	*Totals*
A		0.96	1.40	1.68	1.40	0.96			6.40
B		1.40	3.01	5.47	3.01	1.40			14.29
C		1.68	5.47	44.31	5.47	1.68			58.61
D		1.40	3.01	5.47	3.01	1.40			14.29
E		0.96	1.40	1.68	1.40	0.97			6.41
F	0.96	1.40	2.64	2.80	2.64	1.40	0.96		12.80
G	1.40	3.01	6.87	6.02	6.87	3.01	1.40		28.58
H	1.68	5.47	45.99	10.94	45.99	5.47	1.68		117.22
I	1.40	3.01	6.87	6.02	6.87	3.01	1.40		28.58
J	0.96	1.40	2.64	2.80	2.65	1.40	0.97		12.82
K									
	6.40	20.69	79.30	87.19	79.31	20.70	6.41		300

TABLE 1

Sizes of zones of interaction and of largest individual cell value for each of the distributions of initial adopters in Figure 3.

Figure number: Position of three original adopters.	Number of cells in interaction zone.	Largest value (out of 300) in individual cell.
Figure 3.A: linear arrangement	25	55.25
Figure 3.B: middle cell 1 unit north	23	50.33
Figure 3.C: middle cell 2 units north	21	47.39
Figure 3.D: middle cell 3 units north	19	45.99
Figure 3.E: middle cell 4 units north	17	45.99
Figure 3.F: middle cell 5 units north	15	45.99

choosing judiciously the pattern of initial adopters, the relative space-filling of associated trees might be guided by local municipal authorities so as not to conflict with, or to interfere with, other issues of local concern. The D-values associated with triads of original adopters (as in Table 2) might serve as irreducible elements of this algebra, into which larger sets could be decomposed (much as positive integers (> 1) can be decomposed into a product of powers of prime numbers). The manner in which the decomposition is to take place would

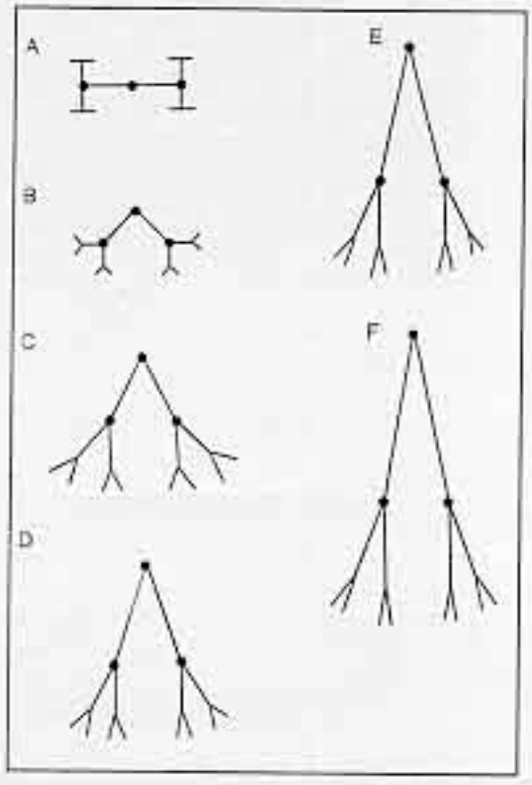

Figure 4.

Fractal trees derived from the diffusion grids of Figure 3; labels A through F correspond in the two Figures. The position of the distribution of original adopters in Figure 3 determines the positions for generators for fractal trees. The interbranch angle, θ, is constant within a tree; values of θ decrease from A. to F. as does the fractal dimension, D.
A. $\theta = 180°$, $D = 2$.
B. $\theta = 90°$, $D \approx 0.72$.
C. $\theta \approx 53.13°$, $D \approx 0.47$.
D. $\theta \approx 36.87°$, $D \approx 0.38$.
E. $\theta \approx 28.07°$, $D \approx 0.33$.
F. $\theta \approx 22.62°$, $D \approx 0.30$.

likely be an issue of considerable algebraic difficulty, no doubt requiring the use of geographic constraints to limit it. (For, unlike the parallel with integer decomposition, this one would seem not to be unique.) An initial direction for such a diffusion–algebra might therefore be to exploit the parallel with the Fundamental Theorem of Arithmetic.

Another use might involve a self-study by the National Center for Geographic Information and Analysis (NCGIA) in order to monitor the diffusion of Geographic Information

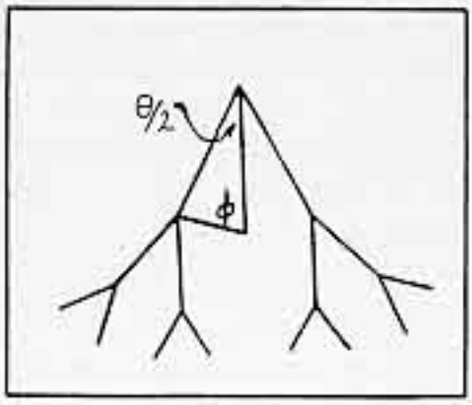

Figure 5. The construction of the angle ϕ used in the calculation of the fractal dimension, D, of the trees in Figure 4.

TABLE 2

D–values, which suggest extent of space–filling, for the trees (Figure 4) representing the patterns of initial adopters in Figure 3.

Figure number: Position of three original adopters.	Size of interbranch angle, θ, in associated tree.	Size of ϕ $= (180 - (\theta/2))$	D–value: $D = (\ln 2)/(\ln(1/\cos\phi))$
Figure 3.A: linear arrangement	Figure 4.A: $\theta = 180°$	45°	2
Figure 3.B: middle cell 1 unit north	Figure 4.B: $\theta = 90°$	67.5°	0.721617
Figure 3.C: middle cell 2 units north	Figure 4.C: $\theta \approx 53.13°$	76.78	0.471288
Figure 3.D: middle cell 3 units north	Figure 4.D: $\theta \approx 36.87°$	80.78	0.378471
Figure 3.E: middle cell 4 units north	Figure 4.E: $\theta \approx 28.07°$	82.98	0.32971
Figure 3.F: middle cell 5 units north	Figure 4.F: $\theta \approx 22.62°$	84.35	0.299116

System (GIS) technology through the various programs designed to promote this technology in the academic arena. University test–sites for the materials of the NCGIA, for example, might be selected as "seeds" with deliberate plans for using a diffusion structure based on these seeds to bring later adopters up to date.

Another use might involve the determination of sites for locally unwanted land uses such as waste sites, prisons, and so forth. Regions expected to experience high concentrations of population coming from the totality of innovations already introduced, or to be introduced, might be overburdened by such a landuse. When relative fractal saturation estimates are run on a computer in conjunction with a GIS, local municipal authorities might examine issues such as this for themselves.

Attraction: the Julia set $z = z^2 - 1$

A different way to view the space–filling characteristics of the diffusion example is to consider each initial adopter as an "attractor" of other adopters, once again suggesting a fractal connection. Viewed broadly, the diffusion example sees adopters attracted to points within an abstract geographic space. The fractal connection is to describe space–filling rather than to describe the pattern or the direction of the attraction. The material below suggests a means of viewing the broad class of spiral geographic phenomena as repelled away from a Julia set toward points of attraction within and beyond the "fractal": hence, pattern and direction of attraction.

The familiar Mandelbrot set, comprising a large central cardioid and circles tangent to the cardioid, along with points interior and exterior to this boundary, is associated with $z = z^2 + c$, where "z" is a complex variable and "c" is a complex constant (Mandelbrot, 1977; Peitgen and Saupe, 1988). When constant values for c are chosen, Julia sets fall out of the Mandelbrot set (Peitgen and Saupe, 1988).

When $c = 0$, the corresponding Julia set is the unit circle centered at the origin. The boundary itself is fixed, as a whole, under the transformation $z \mapsto z^2$, although only the individual point $(1, 0)$ is itself fixed. Points interior to the boundary are attracted to the origin: for them, iteration of the transformation leads eventually to a value of 0. Points outside the circle are attracted toward infinity; the boundary repels points not on it (Peitgen and Saupe, 1988). Various natural associations might be made between this simple Julia set and astronomical phenomena such as orbits or compression within black holes.

When $c = -1$, the corresponding Julia set is described by $z = z^2 - 1$ (Figure 6). The attractive fixed points are 0, -1, and infinity. The repulsive fixed points on the Julia set, found using the "quadratic" formula on $z^2 - z - 1 = 0$, are at distances of $(1 + \sqrt{5})/2$ and $(1 - \sqrt{5})/2$ units from the origin along the real axis (distinguished on Figure 6). Points within the Julia set are attracted alternately to 0 and to -1 as attractive "two–cycle" fixed points; points outside it are attracted to infinity. To see the "two–cycle" effect, iterate the transformation using $z = 1.59$ (located within the Julia set) as the initial value.

$$
\begin{aligned}
1.59 \mapsto 1.5281 \mapsto 1.3350896 \mapsto 0.7824643 \mapsto -0.3877497 \\
\mapsto -0.849650 \mapsto -0.2780946 \mapsto -0.9226634 \mapsto -0.1486922 \\
\mapsto -0.9778906 \mapsto -0.0437299 \mapsto -0.9980877 \mapsto -0.003821 \\
\mapsto -0.9999854 \mapsto -0.0000292 \mapsto -1 \mapsto -0.00000000016 \\
\mapsto -1 \mapsto 0.
\end{aligned}
$$

This value of z is attracted to -1 faster than it is to 0. In this case, iteration strings close down on points of at traction; this is not the case for all Julia sets. The choice of the value of c determines whether or not such strings can escape (Peitgen and Saupe, 1988).

The movement of an initial point toward an attractor, and away from a fixed boundary (as above), suggests a view of this Julia set as an axis: lines from which the movement of points are measured are "axes." Indeed, the repulsive fixed points on this set, located at $((1 + \sqrt{5})/2, 0)$ and $((1 - \sqrt{5})/2, 0)$, might serve as "units." They are the non– zero terms of the coefficients in the generating function for the Fibonacci numbers (thanks to W. Arlinghaus for suggesting this connection to the Fibonacci generating function; Rosen, 1988). For, the nth Fibonacci number, $a_n = a_{n-1} + a_{n-2}$, $a_0 = 0$, $a_1 = 1$, is generated

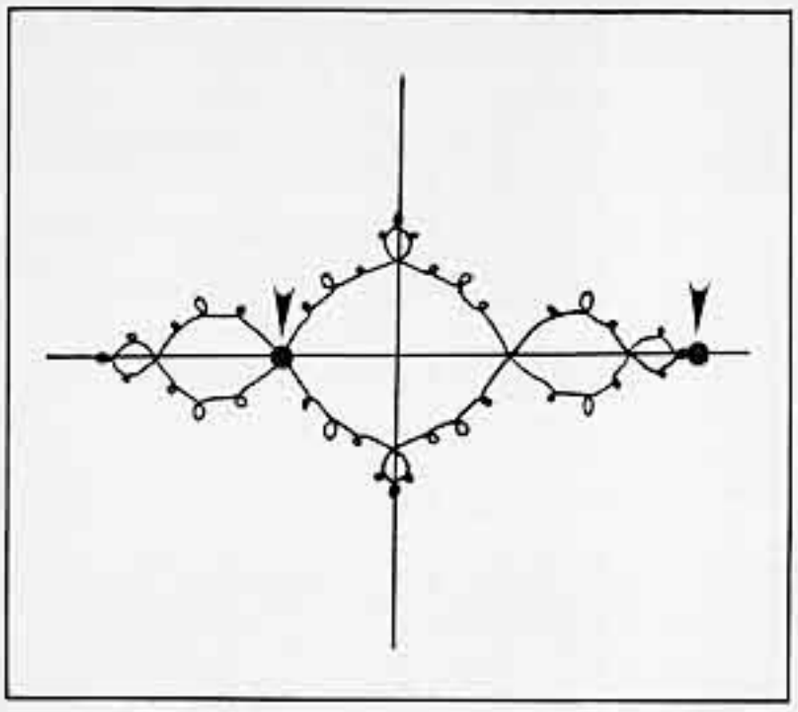

Figure 6.

The Julia set $z = z^2 - 1$. Fixed points $((1 \pm \sqrt{5})/2, 0)$ are distinguished on the boundary.

by

$$a_n = \frac{1}{\sqrt{5}}((1 + \sqrt{5})/2)^n - \frac{1}{\sqrt{5}}((1 - \sqrt{5})/2)^n.$$

Because the Fibonacci sequence can be expressed using the logarithmic spiral, this particular Julia set with these values as "units" might therefore serve as an axis from which to measure spiral phenomena at various scales ranging from the global to the local: from, for example, the climatological to the meteorological.

The mechanics of using this curve as an axis might involve an approach different from that customarily employed. The curve might, for example, be mounted as an equator on the globe partitioning the earth into two pieces in much the way that a seam serves as an equatorial line to partition the hide on a baseball. In this circumstance, there would be freedom to choose how the equator partitions the earth's landmass. It might be located in such a way that exactly half of the earth's water and half of the earth's land lie on either side of the Julia set (using theorems from algebraic topology (Lefschetz, 1949; Dugundji, 1966; Spanier, 1966)).

Beyond the fractal: a graph theoretic connection.

The notions of "attraction" and "repulsion" have also been expressed in the physical world, using graph theory (Harary, 1969; Uhlenbeck, 1960). Fractals rely on distance, angle, or some other quantifier; graphs do not, and in that respect, are more general than are fractals. Fractal–like concepts, such as space–filling and the associated image compression (Barnsley, 1988), may be characterized using graphs, as below (Arlinghaus, 1977; 1985).

This strategy will be expressed in terms of cubic trees (all nodes are of degree three, unless they are at the tip of a branch) of shortest total length (Steiner trees) of maximal branching. It could be expressed in terms of graphs of various linkage patterns; what is important is to begin with some systematic process for forming graphs.

Given a geographic region whose periphery is outlined by landmark positions at P_1, P_2, P_3, P_4, and P_5 (Figure 7.A). View the landmarks as the nodes of a graph and the peripheral outline as the edges linking these nodes (Figure 7.A). A "global" network within the entire pentagonal region might lie along lines of a Steiner (shortest total distance) tree (Figure 7.A) (Arlinghaus, 1977; 1985) attached to the pentagonal hull joining neighboring branch tips (Balaban, *et al.*, 1970).

Figure 7.B will be used as an initial figure from which to produce a network that penetrates triangular geographic subregions (introducing edges P_2P_5 and P_2P_4) more deeply than does the global network of Figure 7.A, yet retains the Steiner characteristic locally within each geographic subregion. An iterative process using Steiner trees (as a "Steiner transformation") will be applied to Figure 7.B (Arlinghaus, 1977; 1983), as follows.

Introduce Steiner networks into each of the three triangular regions and remove the edges P_2P_5 and P_2P_4 so that a new network, containing two quadrangular cells, is hooked into the pentagon $P_1P_2P_3P_4P_5$ (Figure 7.C). Repeat this procedure in the network of Figure 7.C, introducing Steiner networks into all circuits that do not have an edge in common with the pentagon $P_1P_2P_3P_4P_5$. Thus, the two four–sided circuits, $P_5S_1P_2S_2$; $P_2S_2P_4S_3$, in Figure 7.C are replaced with the lines of the network, $P_5S'_1$, $S_1S'_1$, $S'_1S'_2$, $P_2S'_2$, S'_2S_2; $S_2S'_3$, $P_2S'_3$, $S'_3S'_4$, S'_4P_4, S'_4S_3, shown in Figure 7.D. Repeat this process in Figure 7.D, using a Steiner tree, $S_2S''_1$, $S'_2S''_1$, $S''_1S''_2$, S''_2P_2, $S''_2S'_3$, to replace the single four–sided cell, $P_2S'_2S_2S'_3$, not sharing an edge with $P_1P_2P_3P_4P_5$. The result, shown in Figure 7.E, is a tree which cannot be further reduced using the Steiner transformation. It satisfies the initial conditions of generating a tree more local than the Steiner network of maximal branching on $P_1P_2P_3P_4P_5$ (but with local Steiner characteristics), while retaining the global structure of a graph–theoretic tree hooked into $P_1P_2P_3P_4P_5$ in a pattern similar to that of the global Steiner tree (with only local variation as along the edge $S_2S''_1$). This process attempts to integrate local with global concerns. In this case, the process terminates after a finite number of steps; were it to continue, greater space–filling of the geographic region by lines of the network would occur (Arlinghaus, 1977; 1985).

A natural question to ask is whether or not this process necessarily terminates; do successive applications generate a finite reduction sequence of the "cellular" structure into a "tree" structure within $P_1P_2P_3P_4P_5$? Or, is it possible that this transformation, applied iteratively, might fill enough space to choke the entire region with an infinite regeneration of cells and of lines bounding those cells (Arlinghaus, 1977; 1985)?

In this vein, take Figure 7.B and add one edge to it, creating four triangular geographic

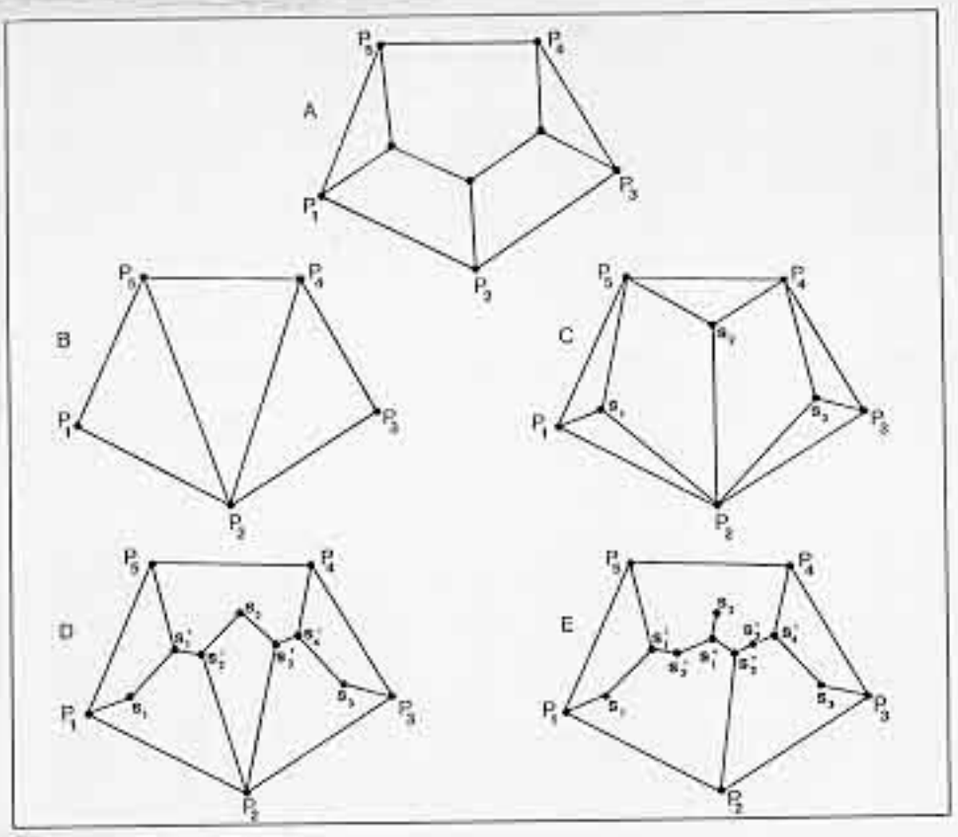

Figure 7.

Network location within geographic regions. Points of the pentagonal hull have "P" as a notational base; Steiner points have "S" as a notational base. A. A Steiner (shortest total distance) tree linking five locations. B. Partition into three distinct, contiguous geographic regions. C. Steiner networks in each geographic region; boundaries separating regions are removed. D. Steiner networks in two quadrangular circuits; circuit boundaries removed. E. Process repeated on remaining quadrangular cell; the result is a tree with local Steiner characteristics that provides global linkage following the basic pattern of the global Steiner tree (Figure 7.A)).

regions (Figure 8.A). Apply the same process to it as above, producing the networks shown in Figures 8.B and 8.C. Clearly, further iteration would simply produce a greater number of polygonal cells, tightly compressed around the node P_2. Discovering a means to calculate

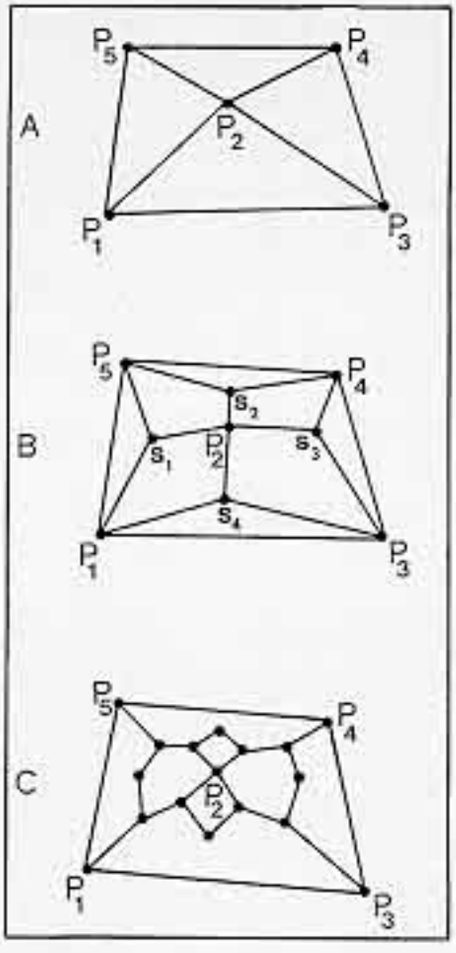

Figure 8.

A modification of Figure 7. An extra edge is added to Figure 7.A, creating a graph-theoretic "wheel." When the procedure displayed in Figure 7 is applied to this initial configuration, cells are added within the hull (B. and C.), rather than removed.

the dimension of this compression is an open issue. It is not difficult, however, to understand under what conditions this sequence might, or might not, terminate (Comments (based on material in Arlinghaus, 1977; 1985) below).

Definition (Harary, 1969; Tutte, 1966),

A wheel W_n of order n, $n > 3$, is a graph obtained from an n-gon by inserting one new vertex, the hub, and by joining the hub to at least two of the vertices of the n-gon by a finite sequence of edges (P_2 is the hub of a wheel formed in Figure 8.A).

Comment 1

Hubs of wheels are invariant, as hubs of wheels, under a sequence of successive applications of the Steiner transformation described above.

Comment 2

Suppose that there exists a finite set of contiguous triangles, T. If T contains a wheel, then a sequence of successive applications of the Steiner transformation to T fails to produce an irreducible tree. The sequence fails to terminate (as long as the Steiner trees produced at each stage are not degenerate).

Comment 3

Suppose that there exists a finite set of contiguous triangles $T = \{L_1 \ldots L_m\}$ with vertex set $V = \{P_1 \ldots P_n\}$, $n > m$ (as in Figure 7.B, $m = 3$, $n = 5$). Suppose that T does not contain a wheel. The number of steps M, in the sequence of successive applications of the Steiner transformation to T required to reduce T to a tree is

$$M = (\max(\text{degree}(P_i))) - 1.$$

Since T does not contain a wheel, it follows from Comment 2 that the reduction sequence is finite. The actual size of M might be found using mathematical induction on the number of cells in T and on the graph-theoretic degree of P_i.

The examples shown in Figures 7 and 8, together with the Comments above, suggest that a sequence of successive applications of the Steiner transformation to such "geo- graphs" resolves scale problems in the same manner as fractals. A natural next step beyond the fractal might be to note that a graph is a simplicial complex of dimension 0 or 1 (Harary, 1969). Thus, similar strategy might be applied there: the triangles of Figure 7.B might represent simplexes of arbitrary dimension in a simplicial complex of higher dimension. Theorems from algebraic topology might then be turned back on the mapping of geographic information using a computer. This notion is already in evidence: because "point," "line," and "area" translate into the topological notions of "0-cell," "1-cell," and "2-cell" in a Geographic Information System, cells in the underlying computerized "sim-pixel" complex can then be colored as "inside" or "outside" a given data set. This follows from the Jordan Curve Theorem (of algebraic topology).

Independent of choice of theoretical tool—from fractal to graph to simplicial complex—the resolution of scale is achieved by uniting local and global mathematical structures: within fractal geometry as well as beyond it.

> "In nature, parts clearly do fit together into real structures, and the parts are affected by their environment. The problem is largely one of understanding. The mystery that remains lies largely in the nature of structural hierarchy, for the human mind can examine nature on many different scales sequentially, but not simultaneously."
>
> *C. S. Smith, in Arthur L. Loeb, 1976.*

References.

Arlinghaus, S. L. 1985. *Essays on Mathematical Geography*. Institute of Mathematical Geography, Monograph #3. Ann Arbor: Michigan Document Services. Arlinghaus, S. L. 1977. "On Geographic Network Location Theory." Unpublished Ph.D. dissertation, Department of Geography, The University of Michigan.

Balaban, A. T.; Davies, R. O.; Harary, F.; Hill, A.; and Westwick, R. 1970. Cubic identity graphs and planar graphs derived from trees. *Journal*, Australian Mathematical Society 11:207-215.

Barnsley, M. 1988. *Fractals Everywhere*. New York: Academic Press.

Boyce, W. E. and DiPrima, R. C. 1977. *Elementary Differential Equations*. New York: Wiley.

Dugundji, J. 1966. *Topology* . Boston: Allyn and Bacon.

Hägerstrand, T. 1967. *Innovation Diffusion as a Spatial Process*. Postscript and translation by Allan Pred. Chicago: University of Chicago Press.

Haggett, P.; Cliff, A. D.; and Frey, A. 1977. *Locational Analysis in Human Geography*. New York: Wiley.

Harary, F. 1969. *Graph Theory*. Reading, MA: Addison–Wesley.

Lefschetz, S. 1949. *Introduction to Topology*. Princeton: Princeton University Press.

Loeb, A. L. 1976. *Space Structures: Their Harmony and Counterpoint*. Reading, MA: Addison–Wesley.

Mandelbrot, B. 1983. *The Fractal Geometry of Nature*. New York: W. H. Freeman.

Peitgen, H.-O. and Saupe, D., editors. 1988. *The Science of Fractal Images*. New York: Springer.

Rosen, K. H. 1988. *Elementary Number Theory and its Applications*. Reading, MA: Addison–Wesley.

Spanier, E. H. 1966. *Algebraic Topology*. New York: McGraw–Hill.

Tutte, W. T. 1966. *Connectivity in Graphs*. London: Oxford University Press.

Uhlenbeck, G. E. 1960. Successive approximation methods in classical statistical mechanics. *Physica* (Congress on Many Particle Problems, Utrecht), 26:17-27.